

Chapter 6

Active Region Part A. Internal Quantum Efficiency in LEDs

Elison Matioli and Claude Weisbuch

In this chapter, we present different techniques used to assess the internal quantum efficiency (IQE) in light emitting diodes (LEDs). The commonly used technique based on temperature-dependent photoluminescence relies in strong assumptions which are discussed in this chapter. We introduce an alternative method to determine IQE based on electroluminescence, in which the external quantum efficiency (EQE) is measured from a single facet of the LED, where the light emission can be calculated with good accuracy. The IQE is ultimately obtained from the ratio of the EQE and the calculated light extraction efficiency. We develop an optical model of the light emission in a multilayered LED structure, from which we derive and validate an approximate model to easily calculate the extraction efficiency through the top facet of any LED structure. We address the various assumptions made to calculate the direct emission model through a single facet and evaluate the effect of photon recycling in the quantum wells. We also calculate the sensitivity of the model to the LED parameters and surface roughness. Finally, we apply this technique to calculate the IQE of both a state-of-the-art and a low performance GaN-based LEDs, highlighting the particular features in each structure.

E. Matioli (✉)

Department of Electrical Engineering and Computer Sciences, Massachusetts Institute of Technology, Cambridge, 02139 MA, USA

e-mail: ematioli@mit.edu

C. Weisbuch

Materials Department, University of California, Santa Barbara, 93106 CA, USA

C. Weisbuch

Laboratoire de Physique de la Matière Condensée, CNRS, Ecole Polytechnique, 91128 Palaiseau, France

6.1 Introduction

The development of the next generation of high efficiency light emitting diodes (LEDs) for solid state lighting requires a quantitative determination of intrinsic device parameters to further performance. A common metric of optoelectronic devices is their output power emitted externally to the device (P_{out}) measured in an integrating sphere. From there, two quantities define the efficiency of the LEDs: the wall-plug efficiency (WPE) η_{wp} i.e., the ratio of electrical input power to optical output power, and the external quantum efficiency (EQE) η_{EQE} , ratio between the number of electrically injected carriers and externally observed photons. The WPE is related to EQE by the voltage drop V at the device due to the diode forward voltage and series resistance, as $\eta_{\text{wp}} = P_{\text{out}}/VI$, where I is the injected current. To optimize it for a given EQE, one requires structures with low contact resistance and high conductivity materials, as well as efficient heat sink to maintain high performance under all operating conditions [1]. η_{EQE} is easily assessed by

$$\eta_{\text{EQE}} = P_{\text{out}}/(\hbar\omega)(I/q)$$

but it only reveals the combination of non-easily separable key parameters, such as carrier injection efficiency η_{inj} , internal quantum efficiency (IQE) η_{IQE} , and light extraction efficiency (LEE) η_{extr} of the LED structure, ratio between the externally emitted photons and the internally generated photons in the active region.

What determines these efficiencies rely on intrinsic and extrinsic properties of materials and architecture of the LEDs. η_{extr} is mainly determined by the LED architecture (such as chip shaping [2], use of patterned substrates [3], photonic crystals [4], surface roughening [5, 6], etc.), with however some dependence on materials parameters (materials absorption, reflection, etc.) (see the chapter by Lalau Keraly et al. in this book); η_{IQE} is mainly connected to the quality of the active layer which is determined by growth conditions such as growth temperature, pressure, quality and flow of precursors, impurity incorporation, as well as growth technique and reactor used, and by the choice of substrate, which affects the crystalline quality, doping profile, defect density of the material, uniformity and surface morphology. It is therefore of great importance to have a precise evaluation of the materials quality as given by η_{IQE} to assess growth quality. This quantity also serves to separately evaluate η_{extr} from η_{EQE} and compare on an absolute scale the various techniques to enhance light extraction.

In addition, the IQE defined by the ratio between the electrically injected carriers and the internally emitted photons, is itself the product of the electron injection efficiency η_{inj} , ratio of carriers injected in the device to those reaching the light emitting regions (usually quantum wells (QWs)) and of the radiative efficiency, η_{rad} , ratio of injected electron-hole (e-h) pairs that recombine radiatively to generate photons and the total number of injected e-h pairs. η_{inj} is mostly determined by the LED heterostructure design, with carrier overflow and QWs uniform injection being examples of phenomena to be controlled.

Equations (6.1) and (6.2) express the relations between these various quantities.

$$P_{\text{out}} = \frac{\hbar\omega}{q} I \eta_{\text{inj}} \eta_{\text{rad}} \eta_{\text{extr}} \quad (6.1)$$

$$\eta_{\text{IQE}} = \eta_{\text{inj}} \eta_{\text{rad}} \quad (6.2)$$

where $\hbar\omega$ is the photon energy and q is the electron charge.

The variations in the measured IQE are expected to be mainly due to η_{rad} , which is directly linked to materials quality, allowing to assess growth quality in a routine fashion, to optimize epitaxial design and to check run to run reproducibility. From Eq. (6.1), the IQE in an LED structure can be written as

$$\eta_{\text{IQE}} = \frac{P_{\text{out}}}{\frac{\hbar\omega}{q} I \eta_{\text{extr}}} = \frac{\eta_{\text{EQE}}}{\eta_{\text{extr}}} \quad (6.3)$$

In the following sections, we present two methods to determine IQE, the first based on photoluminescence (PL) and the second on electroluminescence (EL). To obtain η_{IQE} from the η_{EQE} measurement using Eq. (6.3) a good knowledge of η_{extr} is required, which is not known in a complex LED structure usually containing light extraction features which complicates the precise determination of η_{extr} . The PL-based method circumvents this issue by considering a reference point at low temperature (LT) where η_{IQE} is assumed to be unity, and assuming that η_{extr} is the same at room temperature (RT), any variation between LT and RT is due to the change in η_{EQE} . Thus the η_{IQE} at RT is just the ratio of the η_{EQE} measurements at RT and LT. The EL-based method considers a LED structure with a well defined geometry and without light extractors, such that η_{extr} is known a priori. Then the η_{IQE} is determined from η_{EQE} as $\eta_{\text{EQE}}/\eta_{\text{extr}}$.

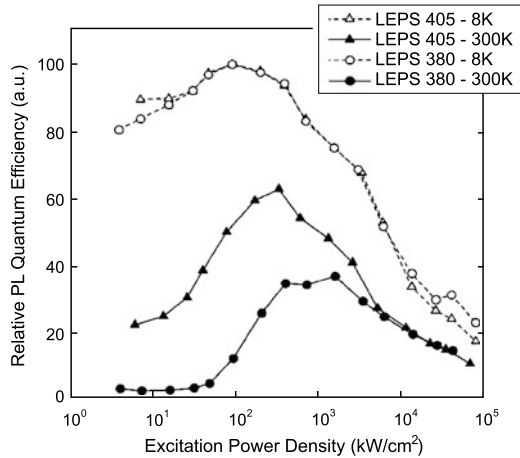
6.2 Assessment of IQE from Photoluminescence Measurements

The IQE is widely estimated by temperature-dependent photoluminescence (PL), in which the intensity of the emitted light at a certain range of PL excitation is measured at low temperature (LT), usually below ~ 10 K and at room temperature (RT). Under the assumption that the IQE at LT is 100 % and that η_{extr} does not change with T , the IQE is estimated from the ratio of the peak PL intensities I_{RT} at RT and I_{LT} at LT.

$$\eta_{\text{IQE}} = \frac{I_{\text{RT}}}{I_{\text{LT}}} \quad (6.4)$$

The assumption that IQE is unity at low temperatures is often made regardless the excitation power density. However the IQE and the PL intensity are themselves dependent on excitation power density [7, 8] at all temperatures, being dominated by Shockley-Read-Hall (SRH), or non-radiative recombination mechanisms at low

Fig. 6.1 [After Watanabe et al. [7]] Relative PL emission normalized by the peak intensity at LT as a function of excitation power density for two different devices at 8 K and 300 K. Note that the PL emission is largely dependent on excitation density and the peak of PL emission occurs at different excitation power densities at LT and RT



excitation density and by Auger recombinations at high excitations [9] (see Fig. 6.1 from Ref. [7]).

A careful procedure is therefore required for estimating the IQE using the temperature-dependent PL method. A large range of excitation power densities, over several orders of magnitude, is needed to correctly determine the peak IQE at low temperature, otherwise the base level that normalizes the low temperature PL intensity at 100 % IQE is incorrect. This procedure is often times not mentioned in the literature [10].

The assumption of unity IQE considers that non-radiative recombination mechanisms are eliminated at low temperatures, which would be justified if only thermally-activated defect-induced recombinations were the dominant non-radiative recombination mechanism. However, Fig. 6.1 shows that non-radiative mechanisms are still present at low excitation density even at low temperatures. The assumption that the peak PL at LT corresponds to 100 % IQE lacks fundamental support.

Another issue is that the peak PL emission occurs at different excitation power densities at LT and RT, and hence to different carrier density in the active region, which makes it difficult to compare these quantities since the competition between SRH, radiative and auger recombinations depend on carrier density.

The IQE determined from PL-based methods also assumes similar carrier injection to the active region compared to electroluminescence. It neglects the effects of applied bias in the internal electric field in the QWs, and also neglects the different carrier injection in individual wells of a MQW structure under PL and EL excitation. In a MQW structure under PL excitation, electron-hole pairs are generated in all QWs, whereas under EL excitation, the carrier distribution in the MQW is, in general, inhomogeneous and dependent on temperature and current density [11, 12]. Laubsch et al. demonstrated a similar behavior of the emission under PL and EL excitation for a single QW structure [8], however the majority of the LEDs fabricated today are based on MQW structures.

These strong assumptions used in the temperature-dependent PL method justify the search for other techniques based on similar operation condition and injection mechanisms as the operating LED.

6.3 Principle of IQE Assessment from Electroluminescence Measurements

As given by Eq. (6.3), P_{out} , or equivalently η_{IQE} , can be measured at a given current, and η_{extr} can be precisely calculated for a simple enough LED geometry. This section is divided in two parts, the first covering the results of calculations of the η_{extr} in a simple LED geometry, with details to be found in Ref. [13] or in the Appendix A of this chapter, and the second covering the fabrication details of a simple LED structure adapted for this method [14], and experimental results.

The small extraction efficiency of planar LED structures originates from the fact that only a small fraction of the photons generated within the active region is directly emitted out of the device at their encounter with interfaces, which corresponds to the fraction of light emitted with its wavevector within the air cone. The majority of the light is emitted outside the air cone and is reflected back in the device. A fraction of such photons is dissipated by material defects, free carriers in doped regions, and absorbing materials (such as metal contacts). Another fraction is absorbed by the active material (light emitting material) in the device which can be re-emitted and may re-attempt to escape the LED structure. This mechanism, called photon recycling is an efficient way to significantly increase extraction efficiency in the LED when both η_{IQE} and the fraction of light recycled are large. This is treated in more details in Sect. 6.5 of this chapter. Photons can also escape the LED through the light cone of any exposed facets after a few bounces within the structure. This mechanism can be very efficient when dissipation mechanisms, including QW re-absorption, are very small along the sometimes long trajectories required to bounce back in the escape angle: suffices to remark that in GaAs LEDs with 2 % direct extraction, tens of bounces are required to extract most of the light [1]. It is the variety of fates for emitted photons that makes the extraction efficiency difficult to quantify, and highly dependent on the LED chip architecture. The light extraction efficiency based on the use of extracting features such as truncated pyramids, roughened surfaces, patterned sapphire substrates, surface photonic crystals is in a way difficult to quantify, as it will depend on the exact description of the LED geometry, including its sidewalls, and on the loss mechanisms within the LED for the various materials and regions. Detailed simulations rely on ray tracing techniques to explore the different trajectories (see the chapter by Lalau Keraly et al. in this book), or on solving full Maxwell's equations by finite-difference time-domain (FDTD) or plane wave expansion [15].

The way to circumvent the difficult analysis of η_{extr} in commonly used LED structures is to rely on a simple LED geometry, with a computable direct light ex-

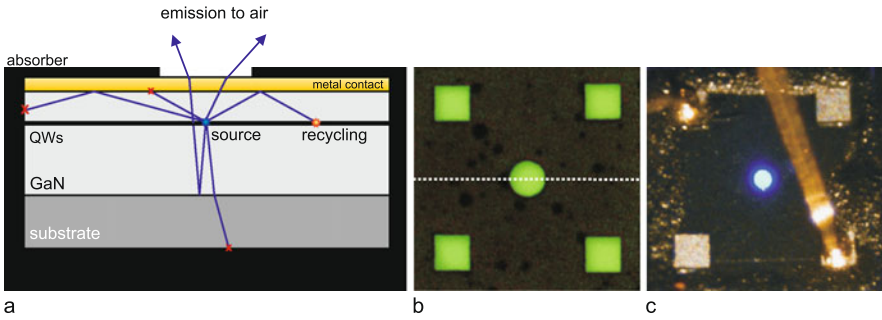


Fig. 6.2 (a) Schematic of a simple geometry LED (contact pads are not shown) surrounded by light absorbing material, along with possible trajectories of the light emitted by the QWs. This view corresponds to the cross-section view at the *dashed-line* in part (b). A small circular aperture allows directly emitted light from the QWs to escape as well as the small fraction reflected off the substrate hetero-interface. Light attempting to escape from sidewalls and backside of the device is dissipated and therefore eliminated from the collected light through the aperture (indicated by *red crosses*). (b) Picture of the absorbing material covering the LED. The *squares* are openings for electric contacts and the *circle* is the aperture for light emission. (c) Picture of the LED covered with absorbing material under bias. Only light emitted through the aperture is observed in air [After Ref. [14]] (Color figure online)

traction, where all other extraction paths are suppressed. This is achieved by covering the LED with a perfectly absorbing material and leaving only a small well-defined aperture of area a on the LED top surface. This is illustrated in Fig. 6.2a, where all trajectories originating from sidewalls, backside of the device, contact pads (not shown), etc., are dissipated by this surrounding material and therefore eliminated from the collected light. Only photons emitted directly from the QW region, plus a small fraction reflected off the substrate hetero-interface (in the case of hetero-structures, for example GaN on sapphire) go through the aperture, and thus reliable estimates of the extraction efficiency η_{extr} can be made. Some care is required when defining the aperture in the absorber material, such as a large spatial separation from the sidewalls and contacts, and a much larger aperture size compared to the GaN thickness L (both roughly larger than $10L$).

The η_{EQE} is measured using an integrating sphere and subsequently corrected by the ratio between the aperture surface a and the total LED top surface A , corresponding to the surface of current injection, as $\eta_{\text{EQE}} = \eta_{\text{EQE}}^{\text{meas}} A/a$, where $\eta_{\text{EQE}}^{\text{meas}}$ is the measured EQE in the integrating sphere. Bringing this technique into practice requires effort in two separate areas. First, we must calculate with good accuracy the light extraction for this device, and evaluate the precision of such model. Second, a device with only direct light extraction as described above must be fabricated.

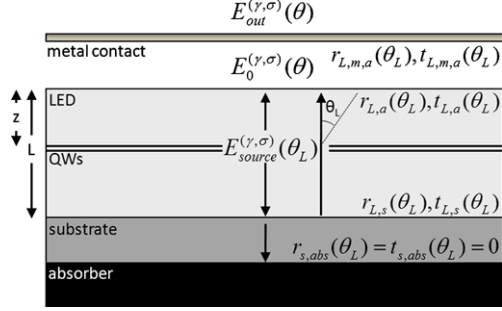
One possible difficulty is that the distribution of light emission from multi-QWs is somewhat involved. QWs in LEDs, usually more than one, are distributed over a finite thickness within the device, and are each few nanometers wide, spaced apart by barrier layers tens of nanometers thick. One might assume that each well is

equally excited and thus emits an equal number of photons in a spherically symmetric pattern. However, it is just as plausible to assume that under EL conditions, either the first well that carriers encounter, the last well (perhaps immediately preceding an electron-barrier layer) or one of the center wells (being most equally accessible to both electrons and holes) would have a disproportionately larger share of the emission. David et al. [12] examined this question with regard to GaN/InGaN LEDs, and reported that nearly all of the emission from an LED comes from the QW nearest to the p -doped side of the device. The predominant emission from the top QW was attributed to the poor hole transfer between QWs, and occurs regardless of the number of quantum wells, often requiring some special design such as a double heterostructure to modify the carrier distribution [12]. That determination was made possible due to the fact that the various QWs have different emission patterns due to their different distances to the interface with an Ag mirror. In our structures comprising materials with only low index contrast, the exact position of emitting QWs will not make any difference as long as they are sufficiently away from the device interfaces with non-nitride materials (see discussion in Appendix B).

For the sake of completeness, Kivisaari et al. [16] proposed an alternative EL-based method to measure the IQE based on extracting the radiative part as the quadratic term of the A - B - C model [17] from the measurements of EQE. The A - B - C model uses as parameter the carrier density in the active region. However, in practice, it is not possible to assess this parameter from the current density injected in the device, especially in the case of multiple quantum wells: this method assumed that all QWs were equally injected with an injection efficiency of 100 % which has been demonstrated to be inaccurate in the nitride system [12]. Their attempt to correct for the uneven injection in each QW, which directly influences the carrier density in each well, was to deliberately consider a thinner active region, replacing the nominal 25 nm by 10 nm without clear theoretical or experimental support, which in turn might lead to an inaccurate estimation of the absolute IQE. Another issue is to assign the quadratic term to radiative recombination only. This is a critical point to the method and this assumption might fail in cases where the injection efficiency is not unity or varies with applied current density. This technique however could have some merit as a relative measurement between batches of similar chips, to assess the origin of variations in efficiency on growth and fabrication quality.

A simple LED geometry on a foreign substrate (the case of LEDs in bulk GaN substrates is treated in Sect. 6.3.2) can be described from an optical point of view as consisting of 3 distinct homogeneous layers: the LED active layer (L), substrate (s), and a thin metal contact (m) in the top surface, as shown in Fig. 6.3. The outer medium is air (a). The structure is surrounded by light absorbing material (abs) which removes all contributions to E_{out} other than the direct propagation of the $E_{\text{source}}^{(\gamma, \rho)}$ upward and its reflection at the LED/substrate interface. Here γ indicates the dipole orientation and ρ the polarization TE and TM. In the analysis presented in Ref. [13] and in Appendix A, we derive a general expression of the electric field in a structure without metal contacts and separately calculate a transmission function corresponding to the absorbing metal, since the electric field is much more sensitive

Fig. 6.3 Schematics of the simple LED geometry consisting of 3 distinct homogeneous layers: the LED (L), substrate (s), and a thin metal contact (m) in the top surface



to the metal parameters, such as thickness and refractive index, than to the LED structure parameters—this is actually the core of our analysis.

The external electric field $E_{\text{out}}^{(\gamma, \rho)}$ is then calculated from the metal transmission function \mathcal{T}_m^ρ and the external electric field of a structure without metal contact $E_0^{(\gamma, \rho)}$, benefiting from a general property of light propagating in stratified planar media [18, 19], described by a matrix formalism, which allows us to separate the effect of the metal contact from the LED as [13] $|E_{\text{out}}^{(\gamma, \rho)}|^2 = \mathcal{T}_m^\rho |E_0^{(\gamma, \rho)}|^2$. From the expression of the electric field emitted to air, we calculate the external power per solid angle $dP_{\text{out}}^{(\gamma, \rho)}(\theta, \lambda)/d\Omega dS$ and the exact extraction efficiency. The complete derivation of these expressions is described in Appendix A and Ref. [13]. The extraction efficiency was then simplified by the following approximations (see Appendix A):

Variable-Incidence (VI) approximation:

$$\eta_{\text{extr}} \simeq \langle \mathcal{T}_m^{\text{TE}} \rangle_{(\lambda, \theta)} \eta_{\text{extr}}^{0, \text{TE}} + \langle \mathcal{T}_m^{\text{TM}} \rangle_{(\lambda, \theta)} \eta_{\text{extr}}^{0, \text{TM}} \quad (6.5)$$

or the *Normal-Incidence (NI) approximation:*

$$\eta_{\text{extr}} \simeq \langle \mathcal{T}_m(0^\circ) \rangle_\lambda \eta_{\text{extr}}^0 \quad (6.6)$$

where $\langle \mathcal{T}_m^\rho \rangle_{(\lambda, \theta)}$ is the metal transmission function averaged in both λ and θ , $\langle \mathcal{T}_m(0^\circ) \rangle_\lambda$ is the metal transmission function averaged over the LED emission wavelengths and η_{extr}^0 is the extraction efficiency of the LED with metal contacts.

6.3.1 Calculation of Light Extraction Efficiency in a Simple GaN-Based LED

The LED structure considered here is the same used in the experimental section of this chapter. The LED material is GaN on a sapphire substrate. The LED thickness is $L = 4869$ nm, the distance z of the top surface to the QW is 140 nm. The central emission wavelength from the QW is 445 nm and the measured refractive

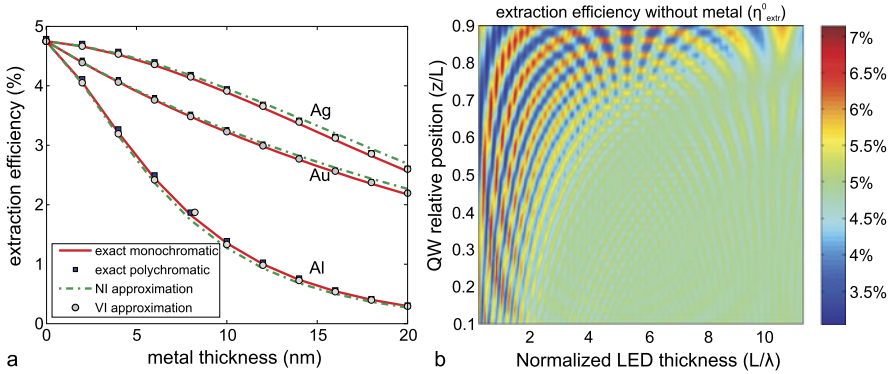


Fig. 6.4 (a) Extraction efficiency of a GaN-based LED on sapphire substrate versus metal thickness for Au, Ag and Al, using the analytical expressions for monochromatic (*solid*) and polychromatic (*squares*) emission, VI (*circle*) and NI (*dashdotted*) approximations. The *center* wavelength was $\lambda = 445$ nm and for the polychromatic emission $\sigma^2 = 25$ nm. (b) Extraction efficiency to air as a function of LED thickness and QW position in the LED (z is relative to the LED top surface)

indexes of the materials at this wavelength are $n_L = 2.475$ and $n_s = 1.779$ for the LED and substrate respectively. The lineshape of the QW was approximated by a symmetric Gaussian function centered at 445 nm with variance $\sigma^2 = 25$ nm, which is typical for InGaN/GaN QWs. We calculated the extraction efficiency versus metal thickness for the common metals: Au, Ag and Al, whose optical constants are $n_{\text{Au}} = 1.544 + i1.896$, $n_{\text{Ag}} = 0.155 + i2.421$ and $n_{\text{Al}} = 0.616 + i5.394$ at $\lambda = 445$ nm were obtained from the literature [20]. We calculated the exact extraction efficiency from this structure considering both mono- and polychromatic radiation from the QWs and compared these results to the VI and NI approximative models, shown in Fig. 6.4a. The approximative models show an excellent agreement to the analytical and polychromatic results for these three different metals presenting very different optical constants, which further validates our approximate models. The details on the evaluation of the approximative model given by Eqs. (6.5) and (6.6) and validation with the exact calculation of the extraction efficiency for a monochromatic and polychromatic light emission are presented in Appendix A.

Figure 6.4b shows the effect of the LED thickness and position of the QWs relative to the top surface of the LED on the calculated extraction efficiency without metal η_{extr}^0 . The extraction efficiency oscillates significantly for an LED structure thinner than $1 \mu\text{m}$ and tends to a fixed value for thicker structures ($L/\lambda > 5$) and for the QWs located far from the bottom interface with the sapphire substrate (this is the case for most of the GaN-on-sapphire LEDs). The fast oscillating behavior of light extraction with LED thickness (also shown in Fig. 6.13a) is averaged in practical LEDs due to thickness fluctuations and polychromatic emission from the source which yields a much smoother function almost independent on LED thickness.

Therefore, the extraction efficiency results shown in Fig. 6.4a can be generally used to assess the IQE for a large range of LED structures other than the one considered in this section. In fact, the calculation of the extraction efficiency is mostly, if not solely, affected by the metal contact properties. The slope of the curves in Fig. 6.4 reflects the sensitivity of these results to thickness variations of the metal contact, where Au and Ag seems to be a better choice than Al. A more detailed investigation of the sensitivity of our model to different metal contacts, presented in Appendix B, shows that the appropriate choice of metal contacts, such as Au for example (see Fig. 6.13 in Appendix B), reduces significantly the dependence of the modelling results on the LED parameters.

6.3.2 Application to LEDs Grown on Bulk GaN Substrates, Complex LED Structures and Lasers

Let us calculate here the extraction efficiency to air η_{extr}^0 for bulk GaN LEDs, which can then be applied to determine the IQE in such structures by using the VI or NI approximations. The external electric field in this case is written in a simple expression, due to the absence of the interface with the substrate, $|E_0^{(Y,\rho)}| = |E_{\text{source}}^{(Y,\rho)}| |t_{L,a}^\rho|$, which also eliminates the oscillations due to the LED cavity on the extraction efficiency. Figure 6.5a shows the η_{extr}^0 for a bulk GaN LED (solid-red) for QWs placed at 140 nm from the top surface. In this case, the absence of the reflection from the substrate reduces slightly the extraction efficiency through the top surface, considering that the bottom interface is covered with absorbing material.

The $\eta_{\text{extr}}^0(\lambda)$ can be easily calculated for bulk LED from a quadratic fit of this curve:

$$\eta_{\text{extr}}^0(\lambda) = -1.493 \times 10^{11} \lambda^2 + 1.860 \times 10^5 \lambda - 5.817 \times 10^{-3} \quad (6.7)$$

For an easy comparison, we plot in the same figure the η_{extr}^0 for a GaN LED on sapphire (dashed-blue), previously calculated.

The extraction efficiency through a simple facet is often approximated by the fraction of solid angle of the air cone, given by $[1 - \cos(\theta_c(\lambda))]/2$, where $\theta_c(\lambda)$ is the critical angle of total internal reflection inside GaN. For comparison to the exact results, we plot the solid angle approximation (dashdotted-green) in Fig. 6.5a, which shows that this simple approximation has a significant error of at least 10 %, which is due to the non-isotropic radiation from the dipole source.

Turning to the impact of various additional structures commonly found in LEDs, we investigate the two most important: superlattices, often grown above the nucleation layer at the substrate interface to improve growth quality, and the confining layers, needed in most laser structures. We leave aside the thin electron blocking layers, commonly used in LEDs, as it would have a smaller optical effect than these two dominant structures. Figure 6.5b shows the effect of the superlattices: even for 40 period superlattices, the relative modification to light extraction remains below

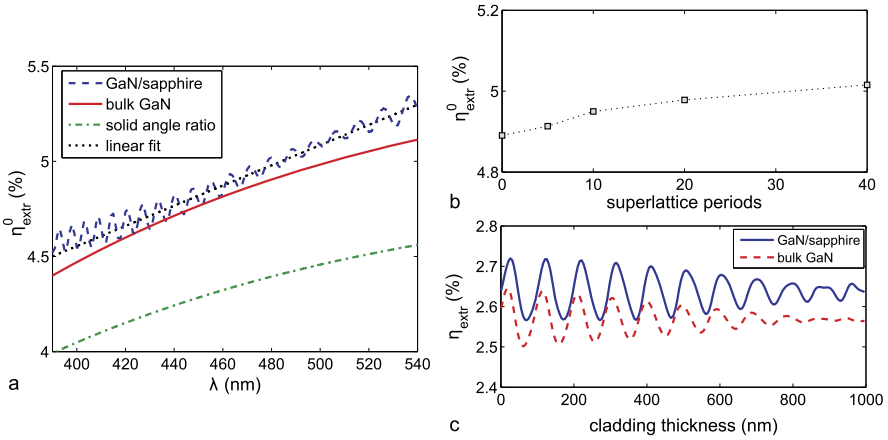


Fig. 6.5 (a) Extraction efficiency η_{extr}^0 for bulk GaN LED (*solid-red*) and for the GaN LED on sapphire previously calculated (*dashed-blue*), for QWs placed at 140 nm from the top surface, along with the solid angle ratio approximation for the extraction efficiency (*dashdotted-green*). (b) Effect of embedded superlattices on the light extraction efficiency to air. We considered a 2 nm-InGaN/2 nm-GaN superlattice below the active region with 0, 5, 10, 20 and 40 periods. (c) Impact of AlGaIn cladding layers thickness on the light extraction efficiency using a 15.4 nm-thick Ni–Au contact and Al content of 15 % in the cladding layer. We considered an active layer (quantum wells, barriers, guiding layers) of fixed 240 nm thickness, sandwiched by two equal cladding layers, for a GaN structure grown on a sapphire substrate (*solid-blue*) or on a bulk GaN (*dashed-red*) (Color figure online)

2 %. Figure 6.5c shows the impact of adding $\text{Al}_{0.15}\text{Ga}_{0.85}\text{N}$ cladding layers of variable thicknesses to an active layer (quantum wells, barriers, guiding layers) of fixed 240 nm thickness over a 4 μm -thick GaN slab on a sapphire substrate (*solid-blue*) or on a bulk GaN (*dashed-red*). The extraction efficiency remains fairly constant in both cases. The rigid downwards shift of 3 % observed when compared to heterostructure is due to the absence of reflection at a substrate interface.

Therefore, the results presented in Fig. 6.4 can be extended to more complex nitride-based LED structures as well as lasers. In the following section we present the combination of this theoretical results with experiments to determine the internal quantum efficiency of LEDs.

6.4 Experimental Assessment of IQE

In the present technique, the LED must be coated with a perfectly light absorbing material containing only a small well-defined aperture on the LED top surface [14] (illustrated in Fig. 6.2a). The aperture diameters varied from 5 to 300 μm to assess the dependence of the total collected light on the aperture size, which is used to feed the theoretical model. The P_{out} from each aperture, for a given current, was measured using an integrating sphere and subsequently corrected by the ratio between

the aperture surface a and the total LED top surface A , corresponding to the surface of current injection. Current was injected by a semi-transparent thin metal layer on the top surface of the LED, through large metallic pads placed far (tens to hundreds of microns) from the circular aperture where the light is collected, to isolate the light measured from optical features with uncertain properties. The IQE was then determined from the following expression:

$$\eta_{\text{IQE}} = \frac{\eta_{\text{EQE}}}{\eta_{\text{extr}}} = \frac{q P_{\text{out}}}{\hbar\omega I} \frac{A}{a} \quad (6.8)$$

where $\hbar\omega$ is the photon energy, q is the electron charge and η_{extr} is the extraction efficiency for a single facet of the LED as calculated in the previous section.

Next sections show the application of such method to a state-of-the-art GaN-based LED as well as to a relatively poor performance device [14].

6.4.1 IQE Measurement of a State-of-the-Art LED

The LED investigated was a state-of-the-art device from Seoul Semiconductors, grown by metal-organic chemical vapor deposition (MOCVD) on a sapphire substrate. The LED structure consisted of a ~ 4670 nm-thick n-GaN followed by 60 nm-thick layer of QWs emitting at $\lambda = 445$ nm and a 140 nm-thick p -GaN layer. The LED top surface was extremely smooth (RMS roughness ~ 0.247 nm for a $5 \times 5 \mu\text{m}^2$ scan measured by atomic force microscope (AFM)), which is an important requirement of the technique. Homogeneous current injection was assured by an annealed semitransparent Ni–Au contact (5/10 nm-thick) of area $A = 484.5 \times 484.5 \mu\text{m}^2$ over the LED top surface. The complex refractive index of the Ni–Au alloy ($n_{\text{alloy}} = 1.4649 + 1.6485i$) was measured from co-deposited and co-annealed films on a sapphire substrate, using variable angle spectroscopic ellipsometry (VASE) [21].

The light absorbing material used was an equal volume mixture of AZ4210 photoresist (PR) and PureBlack carbon black particles (Superior Graphite Corp.). Apertures of 50, 100, 200, and 300 μm diameter were patterned into the absorber by lift-off, where a bilayer of PMGI SF 15 PR followed by AZ4210 was spun onto the surface of the processed LED structure [21].¹ The deposited absorber presented

¹The carbon black particles prevent proper exposure of the PR to UV light, hence it is not possible to pattern this layer using standard photolithography techniques. Instead, a lift-off method was applied, where a bilayer of PMGI SF 15 PR followed by AZ4210 was spun onto the sample surface, on which complete LED structures had already been processed. The AZ4210 was then patterned using standard optical lithography, which acted as a mask for the deep-UV exposure of the PMGI SF 15 layer. This exposed layer was then developed, re-exposed, and developed again, creating a deep undercut in the lift-off mask profile. The mixture of PR and carbon black particles was spun over this patterned lift-off mask and then baked at 200 °C for 1 hour. The baking process caused the mixture to adhere strongly to the sample surface and did not affect the PMGI SF 15, which is robust to temperatures up to 250 °C. The lift-off was completed by placing the sample in 1165 PR stripper at 80 °C for 1 hour with strong sonication.

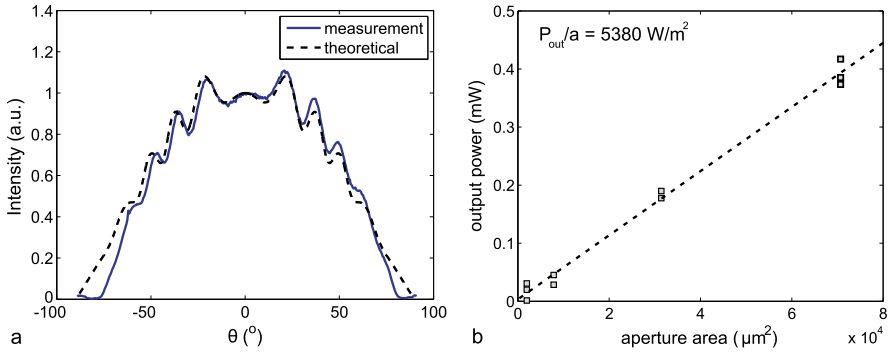


Fig. 6.6 (a) Theoretical (*dashed*) and experimental (*solid*) angle-resolved pattern of the light emission from the LED. (b) Output power emitted from aperture versus aperture area

optical transmissivity of 0.04 % and reflectivity of 0.8 % at normal incidence. The light absorbing material for the backside and sidewalls of the device was flat black paint (Rustoleum). The measured specular reflection at normal incidence for this material was less than 1.5 %, and the total scattered reflection was less than 3 % of incident light from an absorber-air interface, which are suitable for the application envisaged in this work. After coating with absorber, samples were diced, mounted to headers, and wire-bonded for integrating sphere measurements.

As shown in the previous section, the theoretical η_{extr} is readily available for the common metals, such as Ag, Au and Al (Fig. 6.4). The calculation for other metal contacts requires the accurate knowledge of the refractive index of the semitransparent contact $n_{\text{alloy}} = 1.4649 + 1.6485i$, which in this case was done by VASE. The calculated η_{extr} for this device, using the model described in the Appendix A, was 2.7 %. This low value is justified by the rather thick Ni-Au current spreading layer that considerably absorbs the light going to air. As shown in Fig. 6.4a, the calculated η_{extr} is fairly constant for a GaN layer thicker than 1.5 μm , and does not depend on the QW position in the present structure. For the nominal GaN thickness and QW relative position of our structure, the maximum variation in η_{extr} is at most 1.6 % (Appendix B).

As a confirmation of the theoretical predictions, we compared the angular pattern of the light emitted to air from the theoretical model (Eq. (A.18)) to the experimental results (Fig. 6.6). The angular emission from the LED was assessed using an angle-resolved setup, where the far field spectrum was collected at all angles θ from -90° to 90° . The oscillations observed correspond to Fabry-Perot interferences from the GaN interfaces with the substrate and the metal. The excellent match between the experimental and theoretical curves in Fig. 6.6a is an indication of the correct theoretical model used to predict the LED light emission. As explained in Appendix C, a small damping corresponding to an isotropic emission of 1 % of the total output power emitted from the LED ($F_{\text{rough}} = 1\%$) was considered in the theoretical curve. While this improved the agreement between the experimental and theoretical curves, it accounted for light scattering from any small roughness present in

the metal contact. In the following section, we show that the damping included in LEDs with much rougher surfaces (rms roughness of ~ 10 nm for a $5 \times 5 \mu\text{m}^2$ scan measured by AFM) is as high as 70 %, which corroborates the smoothness of the interfaces in the present sample.

The output power of the light emitted from the aperture on the LEDs was measured in an integrating sphere under pulsed excitation, with duty cycle of 0.1 %, to eliminate the degrading effect of heating on the IQE. The measured output power for 50, 100, 200, and 300 μm diameter apertures varied linearly with the aperture area as presented in Fig. 6.6b. The linear variation of the output power versus aperture size validates the use of a homogeneously distributed set of dipoles replacing the QWs in the theoretical model. The power per unit area P_{out}/a deduced from its slope at a nominal input current density of 8.52 A/cm^2 , averaged for several devices, was $5380 \pm 380 \text{ W/m}^2$. This current density corresponds to the peak IQE, which was first determined by measuring the P_{out} versus current density. Using this value in Eq. (6.8) combined to the theoretical η_{extr} of 2.7 % resulted:

$$\eta_{\text{IQE}} = 83.8 \%$$

6.4.2 EL-Based IQE Measurement of a Poor Performing LED: Effect of Surface Roughness

We also applied the present technique in a poor performing LED. The GaN-based LED used in this study was grown by MOCVD on a sapphire substrate, with 5x-InGaN QWs emitting at 445 nm. The LED was processed with a semitransparent Ni–Au contact to the *p*-GaN layer. The LED structure was composed of a 4570 nm-thick GaN over a sapphire substrate. The QWs, emitting at $\lambda = 445$ nm, were below a 295 nm-thick *p*-GaN layer. The index of refraction and effective thickness of the Ni/Au alloy, measured by VASE, was $n_{\text{alloy}} = 1.544 + i1.016$ at $\lambda = 445$ nm and 18.4 nm, respectively. The sapphire substrate was considered infinitely thick because of the assumption that the light going downwards in the sapphire substrate is completely absorbed at the interface of the absorbing material and sapphire. The calculated η_{extr} for this device was 3.03 %, which was different than the previous sample due to differences on the index of refraction and thickness of the Ni/Au alloy. This result also considered a device with a smooth material-to-air interface. The output power varied linearly with aperture area indicating uniform emission across the device surface. The slope of the curve in Fig. 6.7a yields a power per unit area of 2900 W/m^2 at an injection current density of 7.9 A/cm^2 , where the peak EQE occurred. Using Eq. (6.8), the peak IQE of these devices was estimated to be 43 % at a current density of 7.9 A/cm^2 . The IQE value obtained must be carefully considered at this point.

The theoretical model assumes a perfectly flat and smooth surface, however, the device material used had a RMS surface roughness of 10 nm measured by AFM, due to the low temperature growth used for the *p*-type GaN. This rough surface destroys

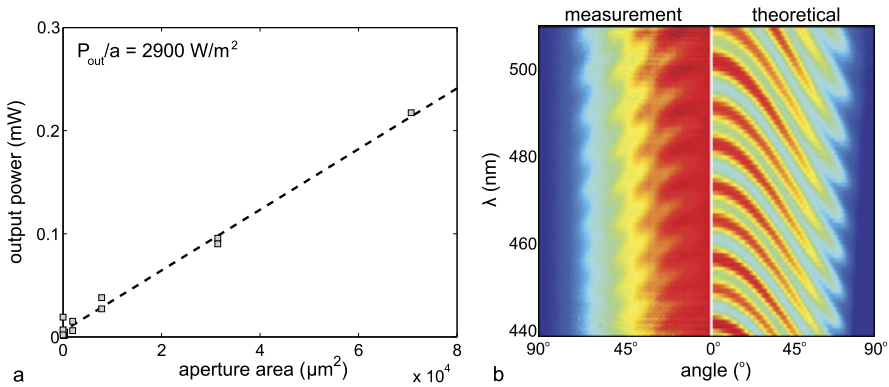


Fig. 6.7 (a) Measured output power versus aperture surface. (b) Angle-resolved measurement on the sample with rough surface (*left*) compared to the calculated emission using the dipole model (*right*). Notice the blurry Fabry Perot fringes from the current sample indicating a pronounced effect of the roughened surface

the constructive interferences in the LED interfaces and enhances the extraction efficiency of the device compared to the calculated value. The ratio between guided light and directly extracted light is not maintained which partially invalidates the results from the theoretical model. Figure 6.7b shows the angle-resolved measurement in this rough LED and the calculated radiation from a similar LED with flat surfaces. The Fabry-Perot fringes are much less pronounced when the LED surface is rough.

To account for this effect, we modelled the effect of the surface roughness as a Lambertian light source emitting simultaneously with the dipoles inside the flat structure, as described in details in the Appendix C. This is justified by considering that the light impinging the rough surface is randomly scattered, corresponding to an isotropic source inside the structure. Let us use this model to account for the surface roughness in our sample. The comparison of the angle-resolved emission between the measurements and dipole model is shown in Fig. 6.8. The blue curve corresponds to the angle-resolved measurement of the LED at $\lambda = 460 \text{ nm}$, which is simply a cross section of the measurement shown in Fig. 6.7b. The red curve corresponds to the calculated emission of the dipoles inside the structure with a perfectly flat surface for the same wavelength, which is far from matching the experimental result shown in blue. However, when the Lambertian emission due to the rough surface, represented by the black curve in Fig. 6.8, is added to the theoretical Fabry-Perot oscillations, it results in the green curve which matches very well the experimental curve. The addition of an amount of Lambertian emission related to the surface roughness to the calculated angular pattern resulted in an excellent agreement to the measurements, validating the dipole model used.

The angle-resolved measurement is therefore a very useful technique to assess the contribution of light randomly scattered to the measured EQE which ultimately can be used to validate the model requirements of flat interfaces. The pronounced oscillations in such measurements fade away proportionally to the presence of light

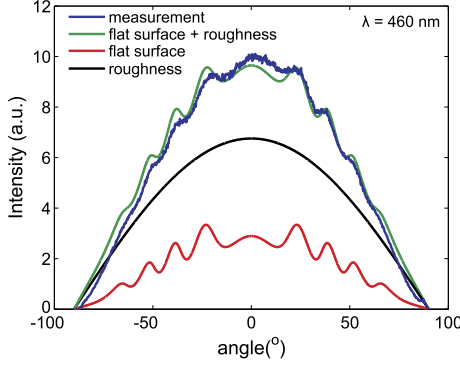


Fig. 6.8 Cross section of the angle-resolved measurement at $\lambda = 460$ nm (blue curve). The red curve represents the calculated emission of the dipoles inside the structure with a perfectly flat surface for the same wavelength. The black curve is the Lambertian emission due to the rough surface and the green curve shows the Lambertian emission added to the theoretical Fabry-Perot oscillations which matches the experimental curve (Color figure online)

scatters in the LED and the accuracy of this model is largely reduced with the presence of such scatterers. The intensity of the Lambertian emission here corresponds to 70 % of the intensity from the measurement. To roughly estimate the IQE, we consider that only the remainder 30 % of the measured P_{out} is due to the emission from dipoles in a flat surface, for which our theoretical extraction efficiency is valid, which results in an estimated IQE of 13 %. However, this should be considered just a rough estimation to account for the effect of surface roughness on the present model, a precise determination of the IQE requires flat smooth interfaces.

6.5 Model for Photon Recycling

In this section we present a simple model to estimate the effect of photon recycling on the extraction efficiency of an LED (Refs. [1, 13, 22]). This mechanism consists of a sequence of re-absorption of the guided light in the LED structure and re-emission by the QWs, that ultimately can play an important role in extracting photons that have not been directly emitted to the air cone in the first pass. The schematic in Fig. 6.9a illustrates the infinite iterations of this mechanism. The η_{EQE} can be written as $\eta_{\text{EQE}} = \eta_{\text{IQE}}\eta_{\text{extr}} + \eta_{\text{IQE}}^2(1 - \eta_{\text{extr}})F_{\text{rec}}\eta_{\text{extr}} + \dots$, therefore, the extraction efficiency with photon recycling is:

$$\eta_{\text{extr}}^{\text{PR}} = \eta_{\text{extr}} \left[1 + \frac{\eta_{\text{IQE}}(1 - \eta_{\text{extr}})F_{\text{rec}}}{1 - \eta_{\text{IQE}}(1 - \eta_{\text{extr}})F_{\text{rec}}} \right] \quad (6.9)$$

where $F_{\text{rec}} = \frac{F_{\text{QW}}}{F_{\text{QW}} + F_{\text{diss}}}$ is the ratio of the LED guided light absorbed by the QWs (F_{QW}) to the total dissipated light ($F_{\text{diss}} + F_{\text{QW}}$).

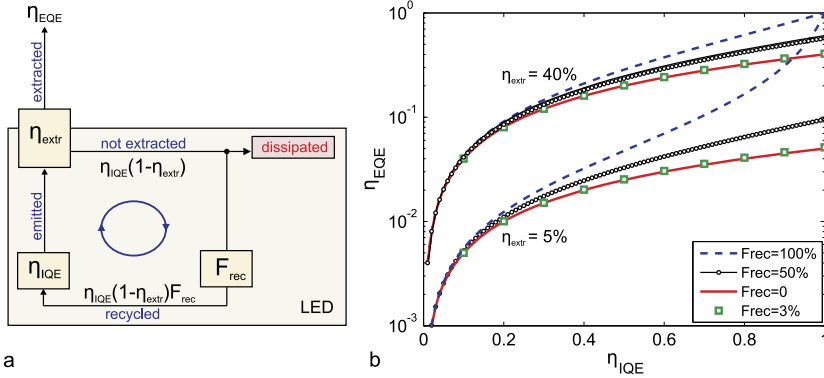


Fig. 6.9 (a) Schematic of the light emitted within the LED structure. (b) Calculated η_{extr}^{PR} versus η_{IQE} for $F_{rec} = 0, 3 \%, 50 \%$ and 100% and for $\eta_{extr} = 5 \%$ and 40%

In the case of nitride-based LEDs, the absorption by QW is spectrally shifted (large Stokes shift) from its emission edge, and only the tail of the absorption curve overlaps the emission spectrum, thus the absorption coefficient is quite small (experimentally estimated in Ref. [23] as 10^3 cm^{-1}). The volume ratio of the QWs to the LED is approximately 1.5% . The absorption coefficient of the metal layer, which is the most significant absorption mechanism in the LED, is approximately $\alpha_m = (4\pi/\lambda)k_m = 5 \times 10^5 \text{ cm}^{-1}$ and the volume fraction penetrated by the guided modes in the metal layer is about 0.2% . Thus, as a rough estimation, $F_{rec} \approx 3 \%$.

Figure 6.9 shows the plot of η_{extr}^{PR} versus η_{IQE} for the cases without, with 50% and 100% photon recycling, as well as the estimated $F_{rec} = 3 \%$ for a nitride-based LED. Two different extraction efficiencies are considered which illustrated both the case of a simple LED geometry ($\eta_{extr} = 5 \%$) as well as a extreme case of an ultra thin microcavity LED ($\eta_{extr} = 40 \%$). In neither of these cases was η_{extr}^{PR} modified by the photon recycling for nitride-based LEDs, due to the very small F_{rec} .

In other material systems, where there is a larger overlap between the absorption and emission energy-edges of the QWs, F_{rec} is much higher and can be close to 100% [1]. In this case, photon recycling is very efficient in increasing the effective extraction efficiency of the LED [24]. This effect is more pronounced when the direct extraction efficiency (without photon recycling) is small. Equation (6.9) provides a corrective factor for the extraction efficiency for material systems such as GaAs where photon recycling is an effective mechanism.

6.6 Conclusions

In this chapter we presented an overview of a few techniques to assess the internal quantum efficiency in LEDs. The IQE is widely estimated by temperature-dependent photoluminescence which relies on strong assumptions, such as that

non-radiative mechanisms are totally eliminated at low temperatures and also similar carrier injection to the active region compared to electroluminescence, neglecting effects of applied bias on the internal electric field in the QWs and different carrier injection in individual wells of a MQW structure under PL and EL excitation.

We presented a technique based on electroluminescence to measure IQE in GaN-based LEDs, which relies on similar operation conditions and injection mechanisms as the operating LED. We derived a model to determine light extraction efficiency, LEE, through a single facet of simple LED structures. The model relies on covering the LED with light absorbing material, which eliminates the difficult-to-model, indirectly extracted light. Thus, the output power, or η_{EQE} , measured in an absolute manner by integrated sphere is only due to directly extracted light, an easily calculated quantity. Applied to GaN structures, the model predicts that the LEE is a product of a bare GaN LED LEE times the transmission function of the top metal contact. General values of the bare LED LEE as $\eta_{\text{extr}}^0(\lambda) = 5.31 \times 10^4 \lambda + 2.43 \times 10^{-2}$ were given, which were quite independent on the details of the LED structure such as exact value of GaN thickness, presence of superlattices or confinement layers, etc. The same is true for LEDs grown over GaN free-standing substrate, with a small modification of $\eta_{\text{extr}}^0(\lambda)$ as one misses the power reflected from the GaN/sapphire interface into the escape cone. The effect of different contact metals on the LEE was investigated, leading to a conclusion that Au-based metal contacts are the best choice, among commonly used metals, for the application of the present technique in terms of LEE robustness to LED parameters.

This model was extended to predict the angular light emission in LEDs, which can be used to compare the theoretical and experimental results as well as to identify the presence of surface roughness which could be detrimental to this model. Photon recycling was evaluated and shown to be negligible in nitride structures, mainly because of the large Stokes shift between emission and absorption.

We also presented the experimental details to fabricate a suitable structure for the application of the present method, consisting of patterning a well-defined aperture in a light absorbing material that surrounds the device. The application of this method to a state-of-the-art GaN LED yielded a peak IQE of 83.8 %. The angle-resolved prediction of the light emitted in the LED from the theoretical model was validated with experimental data and the excellent match between theory and experiments corroborates the model developed.

Acknowledgements The authors would like to thank James Speck for triggering this work, for his continuous interest and many enlightened discussions and Amorette Getty for her large contribution with the experimental part in this work. This material is based upon work partially supported as part of the ‘Center for Energy Efficient Materials’ at UCSB, an Energy Frontier Research Center funded by the U.S. Department of Energy, Office of Science, Office of Basic Energy Sciences under Award Number DE-SC0001009 and by the Department of Energy (DOE) under project No. DE-FC26-06NT42857 and by the Solid State Lighting and Energy Center (SSLEC) at the University of California, Santa Barbara (UCSB).

Appendix A: Theoretical Model of Light Emission in LEDs: QW Emission Described by Classical Dipoles

QWs in LEDs are usually more than one, distributed over a finite thickness within the device, as each is a few nanometers wide and spaced apart by barrier layers of tens of nanometers thick. One might assume that each well is equally excited and thus emits an equal number of photons in a spherically symmetric pattern. However, it is just as plausible to assume that under EL excitation, either the first well that carriers encounter, the last well (perhaps immediately preceding an electron-barrier layer) or one of the center wells (being most equally accessible to both electrons and holes) would have a disproportionately larger share of the emission. David et al. [12] examined this question with regard to GaN/InGaN LEDs, and reported that nearly all of the emission from an LED comes from the QW nearest to the p -doped side of the device. The predominant emission from the top QW was attributed to the poor hole transfer between QWs, and occurs regardless of the number of quantum wells, often requiring some special design such as a double heterostructure to modify the carrier distribution [12]. That determination was made possible due to the fact that the various QWs have different emission patterns due to their different distances to the strongly reflecting Ag/GaN interface.

To address the question of calculating light emission per QW, we refer to Benisty et al. [25], who used dipole emitters as a photon source term in LED emission models. Benisty et al. model the emission from the dipoles as a discontinuity in the scattering matrix propagation technique [26], as we describe below. The use of dipole emitters is justified by the similarity between the normalized expressions of the rate of spontaneous emission in QWs and the power emitted by classic electric dipoles. The rate of spontaneous transitions of e-h pairs between the conduction and valence bands in a QW, given by Fermi's golden rule, is proportional to $\mathcal{M}_{c-v} = |\langle \psi_c | \hat{e} \hat{p} | \psi_v \rangle|^2$, where \hat{e} is the light polarization, \hat{p} is the momentum operator, ψ_c and ψ_v are the conduction and valence band wavefunctions, respectively [27, 28]. The angular dependence of \mathcal{M}_{c-v} is well described by combinations of horizontal and vertical dipole-like terms [29]. The normalized radiation patterns, given by the power per unit of solid angle, of vertical (v) and horizontal (h) dipoles, for both TE and TM polarizations are given by [25]:

$$\frac{dP_{\text{source}}^{(v, TM)}}{d\Omega}(\theta_L) = \frac{3}{8\pi} \sin^2 \theta_L \quad (\text{A.1a})$$

$$\frac{dP_{\text{source}}^{(h, TE)}}{d\Omega}(\theta_L) = \frac{3}{16\pi} \quad (\text{A.1b})$$

$$\frac{dP_{\text{source}}^{(h, TM)}}{d\Omega}(\theta_L) = \frac{3}{16\pi} \cos^2 \theta_L \quad (\text{A.1c})$$

where θ_L is the angle with respect to the vertical direction.

The replacement of the electron-hole excitons by a uniform distribution of dipoles, whose emission is propagated through the multilayered structure by

transfer-matrix formalism, allows the calculation of the electric field in any layer of the structure by propagating the electric field from the dipole layer, which are determined from Eqs. (A.1a)–(A.1c) as

$$E_{\text{source}}^{(\gamma,\rho)}(\theta_L) = \sqrt{\frac{dP_{\text{source}}^{(\gamma,\rho)}}{d\Omega}}(\theta_L) \quad (\text{A.2})$$

for a γ dipole orientation and a ρ polarization.

A.1 Analytical Model for Light Extraction Efficiency

The theoretical assessment of the light extraction efficiency η_{extr} in an LED structure is based on the fraction of the integrated emitted power that exits the LED structure and propagates to air. This is determined from the calculation of the electric field radiated from the QWs, based on the propagation of the dipole electric field throughout the structure. The external power per solid angle $dP_{\text{out}}^{(\gamma,\rho)}/d\Omega dS(\theta)$, in the external direction θ , is given by the flux of the Poynting vector emitted from the dipoles, transmitted through the structure and corrected by the change in solid angle when the medium is changed [25]:

$$\frac{dP_{\text{out}}^{(\gamma,\rho)}}{d\Omega dS}(\theta) = \underbrace{\left(|E_{\text{out}}^{(\gamma,\rho)}(\theta)|^2 \frac{n_{\text{out}} \cos(\theta)}{n_L \cos(\theta_L)} \right)}_{\text{transmitted power from dipoles}} \underbrace{\left(\frac{n_{\text{out}}^2 \cos(\theta)}{n_L^2 \cos(\theta_L)} \right)}_{\text{change in solid angle}} \quad (\text{A.3})$$

where $E_{\text{out}}^{(\gamma,\rho)}$ is the external electric field for a γ dipole orientation and a ρ polarization, n_{out} and n_L are the refractive indexes of the external and LED media, respectively. θ and θ_L are respectively the external and internal angles with respect to the vertical direction. The angles in each medium θ_i , between the vertical and the propagation direction of emitted light, are determined from Snell's law $n_i \cos(\theta_i) = n_j \cos(\theta_j)$. The first term in Eq. (A.3) corresponds to the transmitted power from the dipole source to the external medium, given by the Fresnel transmission coefficient and the second term corresponds to the changes in solid angle from different media, obtained from the derivative of Snell's law.

The light extraction efficiency of the LED through a single facet is given by the ratio of the total output power, calculated from the integration of Eq. (A.3) for θ from 0 to $\pi/2$, to the total emitted power. The total emitted power by the normalized dipole source is unity for dipoles in bulk material. However, the total radiation by the dipole source inside an LED heterostructure is modified by the Purcell factor, which corresponds to the relative change in spontaneous emission from a source within an optical cavity compared to the same source in a bulk material [30]. The Purcell factor depends largely on the position of the QWs relative to the interface between the metallic contact and GaN, as well as on the choice of metal (or more specifically, on

the metal reflectivity), which is treated in more details in Appendix B. Figure 6.13 in Appendix B shows the deviation from unity of the total emitted power by the dipoles for different metals (Al, Au and Ag) versus the distance of the QW to their interface with GaN. A judicious choice of contact metal, such as Au, can largely reduce this dependence and for most of the practical cases as well as for the simple geometry structure treated here, the Purcell factor is close to one and the total emitted power by the dipoles can be approximated to unity (deviation from unity of 2.8 % at most). Figure 6.13 of Appendix B also offers a correction factor in case a different metal is used as contacts.

Therefore, the light extraction efficiency of the LED through its top facet is given by

$$\eta_{\text{extr}} = \int_0^{\frac{\pi}{2}} 2\pi \frac{dP_{\text{out}}^{(\gamma, \rho)}(\theta)}{d\Omega dS} \sin(\theta) d\theta \quad (\text{A.4})$$

summed for $\rho = \text{TE}$ and TM , and $\gamma = v$ and h . The e-HH recombinations in the QWs, in both TE and TM polarizations, can be well described by horizontal electric dipoles. The e-LH recombinations can only be partially described by the combination of horizontal and vertical dipoles and will be neglected at low current injections due to the nondegeneracy of the light hole band at the minimum of energy and to the lower density of states of this energy band [29]. Thus $\gamma = h$. Therefore, the only requirement to determine η_{extr} is to calculate the external electric field $E_{\text{out}}^{(\gamma, \rho)}$, which is treated in the following section.

A.2 Exact Calculation of the Electric Field in a Multilayer Structure

The calculation of the electric field in a multilayer structure is based on the transfer matrix formalism, where a wave $E_{\uparrow} e^{+ik_z z} + E_{\downarrow} e^{-ik_z z}$ is represented by $\begin{pmatrix} E_{\uparrow} \\ E_{\downarrow} \end{pmatrix}$, which is the electric field of the upward and downward plane waves, respectively, and $k_z^i = n_i k_0 \cos(\theta_i)$ in the medium i .

In a multilayer structure, the source electric field is propagated through the structure by multiplying it to propagation M_{prop} matrices in the homogeneous layers and interface M_{interf} matrices in the interface between two different media. A convenient property of this method is that an equivalent matrix \mathcal{M} for the entire structure can be simply obtained by multiplying all the interface and propagation matrices corresponding to the structure (Fig. 6.10), as

$$\mathcal{M} = \dots M_{\text{interf}}^{i+1, i} M_{\text{prop}}^i M_{\text{interf}}^{i, i-1} \dots \quad (\text{A.5})$$

The propagation matrix from z_1 to z_2 in a homogeneous medium is:

$$M_{\text{prop}} = \begin{bmatrix} e^{i(k_z(z_2 - z_1))} & 0 \\ 0 & e^{-i(k_z(z_2 - z_1))} \end{bmatrix} \quad (\text{A.6})$$

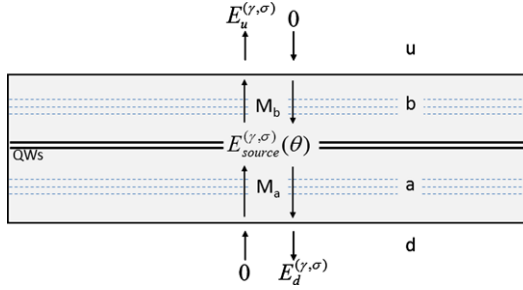


Fig. 6.10 Schematic of a the propagation of the electric fields in a multilayer structure. The external electric fields E_u and E_d , from the top and bottom media, are propagated to the source, where the discontinuity from the source electric field is applied. The matrices M_a and M_b correspond to the transfer matrix of the *bottom* (a) and *top* (b) halves of the LED structure

The interface matrices for TE and TM polarizations are given by

$$M_{\text{interf}}^{\text{TE}} = \begin{bmatrix} \frac{k_z^{(2)} + k_z^{(1)}}{2k_z^{(2)}} & \frac{k_z^{(2)} - k_z^{(1)}}{2k_z^{(2)}} \\ \frac{k_z^{(2)} - k_z^{(1)}}{2k_z^{(2)}} & \frac{k_z^{(2)} + k_z^{(1)}}{2k_z^{(2)}} \end{bmatrix}, \quad M_{\text{interf}}^{\text{TM}} = \begin{bmatrix} \frac{n_2^2 k_z^{(1)} + n_1^2 k_z^{(2)}}{2n_1 n_2 k_z^{(2)}} & \frac{-n_2^2 k_z^{(1)} + n_1^2 k_z^{(2)}}{2n_1 n_2 k_z^{(2)}} \\ \frac{-n_2^2 k_z^{(1)} + n_1^2 k_z^{(2)}}{2n_1 n_2 k_z^{(2)}} & \frac{n_2^2 k_z^{(1)} + n_1^2 k_z^{(2)}}{2n_1 n_2 k_z^{(2)}} \end{bmatrix} \quad (\text{A.7})$$

To obtain analytical expressions for the electric field in the outer media, we impose, as boundary condition of this problem, that the electric field of the incoming waves in the outer media are zero (Fig. 6.10). The external electric fields, from the top and bottom media, are then propagated to the source, where the discontinuity from the source is applied as

$$\mathcal{M}_b \begin{pmatrix} E_u^{(\gamma,\rho)} \\ 0 \end{pmatrix} - \mathcal{M}_a \begin{pmatrix} 0 \\ E_d^{(\gamma,\rho)} \end{pmatrix} = \begin{pmatrix} E_{\text{source}}^{(\gamma,\rho)}(\theta) \\ E_{\text{source}}^{(\gamma,\rho)}(\theta) \end{pmatrix} \quad (\text{A.8})$$

where

$$\mathcal{M}_a = \begin{bmatrix} a_{11} & a_{12} \\ a_{21} & a_{22} \end{bmatrix} \quad \text{and} \quad \mathcal{M}_b = \begin{bmatrix} b_{11} & b_{12} \\ b_{21} & b_{22} \end{bmatrix} \quad (\text{A.9})$$

are calculated from Eq. (A.5) for the bottom (a) and top (b) halves of the LED structure (Fig. 6.10). The electric fields in the top (u) and bottom (d) outer media are

$$E_u^{(\gamma,\rho)}(\theta) = E_{\text{source}}^{(\gamma,\rho)} \frac{\frac{1}{b_{11}}(1 + \frac{a_{12}}{a_{22}})}{1 - \frac{b_{21} a_{12}}{b_{11} a_{22}}} \quad \text{and} \quad E_d^{(\gamma,\rho)}(\theta) = E_{\text{source}}^{(\gamma,\rho)} \frac{\frac{1}{a_{22}}(1 + \frac{b_{21}}{b_{11}})}{1 - \frac{b_{21} a_{12}}{b_{11} a_{22}}} \quad (\text{A.10})$$

In the case of the simple geometry considered in this chapter, the matrix terms are

$$\frac{1}{b_{11}} = \frac{2k_z^b}{k_z^b + k_z^u} e^{ik_z^b L_b} \quad \text{and} \quad \frac{1}{a_{22}} = \frac{2k_z^a}{k_z^a + k_z^d} e^{ik_z^a L_a} \quad (\text{A.11})$$

which correspond to transmission coefficients and

$$\frac{b_{21}}{b_{11}} = \frac{k_z^b - k_z^u}{k_z^b + k_z^u} e^{2ik_z^b L_b} \quad \text{and} \quad \frac{a_{12}}{a_{22}} = \frac{k_z^a - k_z^d}{k_z^a + k_z^d} e^{2ik_z^a L_a} \quad (\text{A.12})$$

corresponding to reflection coefficients.

The electric field after the metal layer can be written as

$$\begin{aligned} E_{\text{out}}^{(\gamma, \rho)} &= \frac{E_{\text{source}}^{(\gamma, \rho)} t_{L, m, a}^\rho e^{i\phi'} (1 + r_{L, s}^\rho e^{i2(\phi - \phi')})}{1 - r_{m, L, a}^\rho r_{L, s}^\rho e^{i2\phi}} \\ &= \frac{E_{\text{source}}^{(\gamma, \rho)} t_{L, a}^\rho e^{i\phi'} (1 + r_{L, s}^\rho e^{i2(\phi - \phi')})}{1 - r_{L, a}^\rho r_{L, s}^\rho e^{i2\phi}} \frac{1 - r_{L, a}^\rho r_{L, s}^\rho e^{i2\phi} t_{L, m, a}^\rho}{1 - r_{m, L, a}^\rho r_{L, s}^\rho e^{i2\phi} t_{L, a}^\rho} \end{aligned} \quad (\text{A.13})$$

The first term is the external electric field without metal contacts and the second is the metal transmission function. Using the general property: $x, y \in \mathbb{C}$, $|xy|^2 = |x|^2|y|^2$, we obtain [13]:

$$|E_{\text{out}}^{(\gamma, \rho)}|^2 = \mathcal{T}_m^\rho |E_0^{(\gamma, \rho)}|^2 \quad (\text{A.14})$$

Let us first calculate the external electric field $E_0^{(\gamma, \rho)}$ in a structure without metal contact. Let the total LED thickness be L and the position of the dipole source within the LED be z . The corresponding phase shifts in the LED are $\phi(\theta_L) = n_L k_0 L \cos(\theta_L)$ and $\phi'(\theta_L) = n_L k_0 z \cos(\theta_L)$, where $k_0 = 2\pi/\lambda$, λ is the wavelength of the emitted light, n_L and θ_L are the refractive index and angle in the LED layer respectively. The transmission and reflection coefficients for a polarization ρ , at each interface from a medium i to j , are given respectively by $t_{i, j}^\rho$ and $r_{i, j}^\rho$.

The external electric field can be determined from the propagation of the dipole electric field $E_{\text{source}}^{(\gamma, \rho)}$ [18]:

$$\begin{aligned} E_0^{(\gamma, \rho)}(\theta) &= E_{\text{source}}^{(\gamma, \rho)} e^{i\phi'} t_{L, a}^\rho (1 + r_{L, a}^\rho r_{L, s}^\rho e^{2i\phi} + \dots) \\ &\quad + E_{\text{source}}^{(\gamma, \rho)} e^{i(2\phi - \phi')} r_{L, s}^\rho t_{L, a}^\rho (1 + r_{L, a}^\rho r_{L, s}^\rho e^{2i\phi} + \dots) \end{aligned} \quad (\text{A.15})$$

$$E_0^{(\gamma, \rho)}(\theta) = \frac{E_{\text{source}}^{(\gamma, \rho)} t_{L, a}^\rho e^{i\phi'} (1 + r_{L, s}^\rho e^{i2(\phi - \phi')})}{1 - r_{L, a}^\rho r_{L, s}^\rho e^{i2\phi}}$$

We recall the transmission and reflection expressions for both TE and TM polarizations for a plane wave going from a medium i to j :

$$\begin{aligned} r_{i, j}^{\text{TE}} &= \frac{n_i \cos(\theta_i) - n_j \cos(\theta_j)}{n_i \cos(\theta_i) + n_j \cos(\theta_j)}, & r_{i, j}^{\text{TM}} &= \frac{n_i \cos(\theta_j) - n_j \cos(\theta_i)}{n_i \cos(\theta_j) + n_j \cos(\theta_i)} \\ t_{i, j}^{\text{TE}} &= \frac{2n_i \cos(\theta_i)}{n_i \cos(\theta_i) + n_j \cos(\theta_j)}, & t_{i, j}^{\text{TM}} &= \frac{2n_i \cos(\theta_i)}{n_j \cos(\theta_i) + n_i \cos(\theta_j)} \end{aligned}$$

The transmission function \mathcal{T}_m^ρ for the metal contact is a simple replacement of the transmission and reflection coefficients of a simple LED/air interface (L, a) with those of an LED/metal/air interface (L, m, a). It contains all the metal parameters separated from the more general expression of $E_0^{(\gamma, \rho)}(\theta)$ and it is written as

$$\mathcal{T}_m^\rho = \left| \frac{1 - r_{L,a}^\rho r_{L,s}^\rho e^{i2\phi}}{1 - r_{m,L,a}^\rho r_{L,s}^\rho e^{i2\phi}} \frac{t_{L,m,a}^\rho}{t_{L,a}^\rho} \right|^2 \quad (\text{A.16})$$

where now $r_{L,m,a}^\rho$ and $t_{L,m,a}^\rho$ accounts for the complex refractive index $\tilde{n}_m = n_m + ik_m$ and thickness t_m of the metal layer as in a homogeneous film [18]:

$$r_{L,m,a}^\rho = \frac{r_{L,m}^\rho + r_{m,a}^\rho e^{i\beta}}{1 + r_{L,m}^\rho r_{m,a}^\rho e^{i2\beta}}, \quad t_{L,m,a}^\rho = \frac{t_{L,m}^\rho t_{m,a}^\rho e^{i\beta}}{1 + r_{L,m}^\rho r_{m,a}^\rho e^{i2\beta}} \quad (\text{A.17})$$

where $\beta = k_0 \tilde{n}_m t_m \cos(\theta_m)$. Therefore, the external field after the metal contact is calculated using Eqs. (A.15) and (A.16) in Eq. (A.14).

The angular dependence of the external power per solid angle can be directly calculated as

$$\frac{dP_{\text{out}}^{(\gamma, \rho)}}{d\Omega dS}(\theta) = \mathcal{T}_m^\rho(\theta) |E_0^{(\gamma, \rho)}(\theta)|^2 \frac{n_{\text{out}}^3 \cos(\theta)^2}{n_L^3 \cos(\theta_L)^2} \quad (\text{A.18})$$

This equation predicts the angular emission of the LED which is used to corroborate the theoretical and experimental results, as shown in later sections. The light extraction efficiency from the top surface in such structure is then calculated using Eq. (A.4), which can be easily done numerically.

A.3 Model for Light Extraction in a Simple LED Geometry

The analytical model presented in the previous section considered a monochromatic emission from the dipoles, but the QW emission in practical LEDs has a broad spectrum (typically 5–10 % of the central wavelength). In this section, the spectral broadening of the source is considered and, while the results are not much different from the monochromatic model, it allows us to simplify the analytical model for η_{extr} .

The effect of the QW lineshape is included in the previous model by averaging the extraction efficiency at different wavelengths with the normalized spectral emission $s(\lambda)$ from the QWs as $\eta_{\text{extr}}^{\text{poly}} = \int_0^\infty s(\lambda) \eta_{\text{extr}}(\lambda) d\lambda$.

The QW spectral emission can be approximated by a Gaussian function $s(\lambda) = \frac{1}{\sqrt{2\pi}\sigma^2} e^{-\frac{(\lambda-\lambda_c)^2}{2\sigma^2}}$ and the asymmetry of its lineshape can be taken into account by combining two Gaussian functions, with different variances σ^2 , at their central

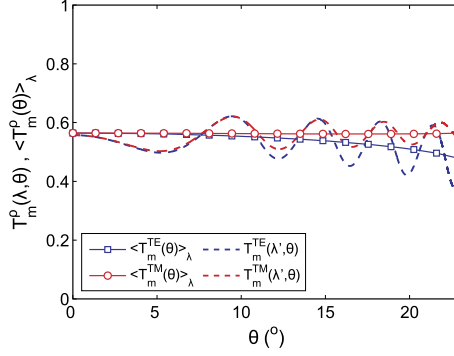


Fig. 6.11 Plot of $\mathcal{T}_m^\rho(\theta)$ for θ within the air cone ($\theta < \theta_c$) and $\lambda' = 445$ nm for TE (*dashdotted*) and TM (*dotted*), along with the plot of the averaged $\langle \mathcal{T}_m^\rho(\theta) \rangle_\lambda$ for TE (*squares*) and TM (*circles*) polarizations. The structure is composed of a 4869 nm-thick GaN-based LED over a sapphire substrate, and the QWs are 140 nm below the top surface. The 15.4 nm-thick metal contact is Ni–Au alloy with experimentally determined optical properties [14]

wavelength. The polychromatic extraction efficiency is thus explicitly written as

$$\eta_{\text{extr}}^{\text{poly}} = \sum_{\rho=\text{TE, TM}} \int_0^\infty s(\lambda) \int_0^{\frac{\pi}{2}} 2\pi \mathcal{T}_m^\rho(\theta, \lambda) \frac{dP_0^{(\gamma, \rho)}(\theta, \lambda)}{d\Omega dS} \sin(\theta) d\theta d\lambda \quad (\text{A.19})$$

where $dP_0^{(\gamma, \rho)}(\theta, \lambda)/d\Omega dS$ is the external power per unit of solid angle of a structure without metal contacts and its dependence with λ is due to Fabry-Perot interferences on the interfaces of the LED layer, which is generally not very pronounced in most of LED structures (thick LED structures), allowing us to make the following approximation [13]:

$$\eta_{\text{extr}}^{\text{poly}} \simeq \sum_{\rho=\text{TE, TM}} \int_0^{\frac{\pi}{2}} \underbrace{\left[\int_0^\infty s(\lambda) \mathcal{T}_m^\rho(\theta, \lambda) d\lambda \right]}_{\langle \mathcal{T}_m^\rho(\theta) \rangle_\lambda} 2\pi \frac{dP_0^{(\gamma, \rho)}(\theta, \bar{\lambda})}{d\Omega dS} \sin(\theta) d\theta \quad (\text{A.20})$$

for a fixed $\bar{\lambda}$ and only the metal transmission function is averaged with respect to λ . The averaged function $\langle \mathcal{T}_m^\rho(\theta) \rangle_\lambda$ varies very slowly with θ for both TE and TM polarizations (an example is shown in Fig. 6.11). This is because the reflection and transmission coefficients do not vary much for θ_L inside the air cone, which is small in the case of high refractive index semiconductors, such as GaN and GaAs. Thus we can approximate Eq. (A.20) by a *Variable-Incidence (VI) approximation*:

$$\eta_{\text{extr}} \simeq \langle \mathcal{T}_m^{\text{TE}} \rangle_{(\lambda, \theta)} \eta_{\text{extr}}^{0, \text{TE}} + \langle \mathcal{T}_m^{\text{TM}} \rangle_{(\lambda, \theta)} \eta_{\text{extr}}^{0, \text{TM}} \quad (\text{A.21})$$

where $\langle \mathcal{T}_m^\rho \rangle_{(\lambda, \theta)}$ is the metal transmission function averaged in both λ and θ .

A simpler expression can be obtained by noticing that the averaged function $\langle \mathcal{T}_m^\rho(\theta) \rangle_\lambda$ is nearly constant inside the air cone for both TE and TM polariza-

tions (Fig. 6.11). Moreover, its value at $\theta = 0^\circ$ is the same for both polarizations $\langle \mathcal{T}_m^{\text{TE}}(0^\circ) \rangle_\lambda = \langle \mathcal{T}_m^{\text{TM}}(0^\circ) \rangle_\lambda = \langle \mathcal{T}_m(0^\circ) \rangle_\lambda$ (reflection and transmission coefficients are equal for both polarizations at normal incidence), thus we obtain the *Normal-Incidence (NI) approximation*:

$$\eta_{\text{extr}} \simeq \langle \mathcal{T}_m(0^\circ) \rangle_\lambda \eta_{\text{extr}}^0 \quad (\text{A.22})$$

Notice that we started calculating the polychromatic extraction efficiency but ended with expressions for the monochromatic extraction efficiency. The spectrally averaged transmission function $\langle \mathcal{T}_m(0^\circ) \rangle_\lambda$ is numerically calculated as

$$\langle \mathcal{T}_m(0^\circ) \rangle_\lambda = \sum_{\lambda=\lambda_1}^{\lambda_2} \mathcal{T}_m(0^\circ, \lambda) \frac{1}{\sqrt{2\pi\sigma^2}} e^{-\frac{(\lambda-\lambda_c)^2}{2\sigma^2}} \Delta\lambda \quad (\text{A.23})$$

where $\Delta\lambda = \frac{(\lambda_2-\lambda_1)}{n-1}$, n is the number of discrete values of λ and the interval $[\lambda_1, \lambda_2]$ needs to be at least a few times larger than σ^2 .

The determination of the extraction efficiency of any LED structure is very simple using one of the two approximative models above. The monochromatic extraction efficiency for the LED structure with metal contacts for any wavelength is simply obtained from the multiplication of the averaged transmission function of the metal, averaged also in the air cone or at $\theta = 0^\circ$, and the monochromatic extraction efficiency of the LED without metal contact (η_{extr}^0).

η_{extr}^0 is not very sensitive to the LED parameters in this simple LED geometry (treated in Appendix B), which can be generally calculated for any LED structure for a given material. The most sensitive parameters in these models are those from the metal, which are contained solely in the metal transmission function \mathcal{T}_m^ρ and can be separately calculated using Eq. (A.16). In the following section, we apply these models to the case of a GaN-based LED.

A.4 Determination of the Extraction Efficiency:

Evaluation of η_{extr}^0 , $\mathcal{T}_m^\rho(\theta, \lambda)$ and $\langle \mathcal{T}_m(0^\circ) \rangle_\lambda$

Let us evaluate the terms $\mathcal{T}_m^\rho(\theta, \lambda)$, $\langle \mathcal{T}_m(0^\circ) \rangle_\lambda$ and η_{extr}^0 and compare the results of the extraction efficiency η_{extr} from the approximative models (Eqs. (A.21) and (A.22)) with the analytical model (Eq. (A.18)) to validate our approximations.

The transmission function $\mathcal{T}_m(\theta, \lambda)$ was averaged using Eq. (A.23) to obtain the approximative models (Eqs. (A.21) and (A.22)), for which the main assumption was that $\langle \mathcal{T}_m^\rho(\theta) \rangle_\lambda$ varied slowly with θ for both TE and TM polarizations. The evaluation of such function for the case of the GaN LED, for both polarizations, is presented in Fig. 6.11, which shows the plot of $\mathcal{T}_m^\rho(\theta)$ for a fixed $\lambda' = 445$ nm for TE (dashdotted) and TM (dotted), as well as the averaged $\langle \mathcal{T}_m^\rho(\theta) \rangle_\lambda$ for TE (squares) and TM (circles) polarizations, for θ within the air cone. The oscillations with respect

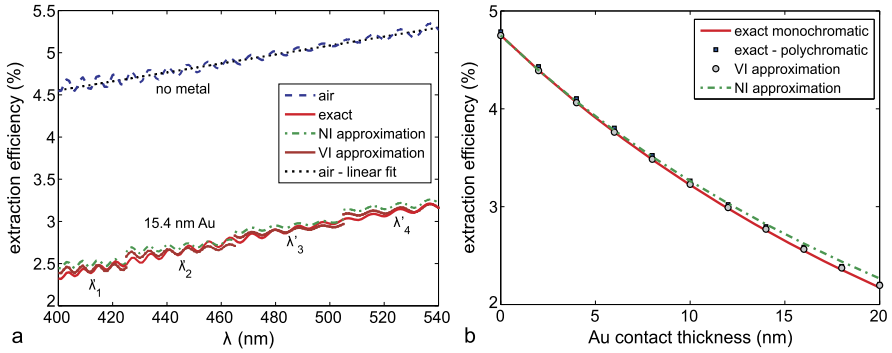


Fig. 6.12 (a) Extraction efficiency of the GaN LED structure versus wavelength using the analytical (*solid-red*), variable-incidence (VI) (*cross-brown*) and normal-incidence (NI) (*dash-dot-green*) approximations along with the extraction efficiency to air (*dotted-blue*) and its linear fit (*dashed-black*). The structure is composed of a 4869 nm-thick GaN-based LED over a sapphire substrate, and the QWs are 140 nm below the top surface. The 15.4 nm-thick metal contact is Ni–Au alloy with optical properties determined experimentally. Four different emission wavelengths were considered, $\lambda'_1 = 405$ nm, $\lambda'_2 = 445$ nm, $\lambda'_3 = 485$ nm and $\lambda'_4 = 525$ nm in the function $s(\lambda)$ to evaluate the approximative models. (b) Extraction efficiency of the GaN LED structure versus metal thickness using the analytical with a monochromatic (*solid*) and polychromatic (*squares*) emission, VI (*circle*) and NI (*dashdotted*) approximations (Color figure online)

to λ observed in $T_m^p(\theta)$ are completely eliminated when this function is averaged with the lineshape of the QWs. As a matter of fact, the averaged function is nearly constant for both polarizations, within the air cone, which supports both approximations made to obtain Eqs. (A.21) and (A.22). This is due to the weak variation of the reflection and transmission coefficients inside the air cone which, in its turn, is small in the case of high refractive index semiconductors, such as GaN and GaAs.

Let us now calculate the extraction efficiency to air η_{extr}^0 (without metal contact) for the GaN LED treated here, which is shown in Fig. 6.12a (dashed line). The small oscillations in extraction efficiency to air with λ for a monochromatic emission average out in real devices with polychromatic (poly) emission—note that the oscillation period in this example is around 7 nm, which is substantially less than the typical 25 nm EL linewidth for blue GaN-based LEDs. As shown later, the extraction efficiency to air, through the top surface of the LED, depends weakly on the LED ‘fine’ structure (for a simple LED geometry), therefore we can determine a general extraction efficiency to air for GaN LEDs grown in sapphire substrates by a linear fit of η_{extr}^0 , which is represented by the dashed line in Fig. 6.12a:

$$\eta_{\text{extr}}^0(\lambda) = 5.31 \times 10^{-4} \lambda + 2.43 \times 10^{-2} \quad (\text{A.24})$$

To validate the models, we calculate the extraction efficiency of the GaN LED structure using the analytical model (Eq. (A.18)) and compare the results to the ones from the approximative models.

The extraction efficiency of the GaN LED structure after the metal contact (η_{extr}) versus wavelength calculated using the analytical model is shown in the solid-red

curve in Fig. 6.12a, along with the results of the VI (cross-brown) and the NI (dashdotted-green) approximations. Four different emission wavelengths were considered in this plot, $\lambda' = 405, 445, 485$ and 525 nm, which were used in the function $s(\lambda)$ to evaluate the approximative models.

The application of both models for same structure when the metal thickness is varied is shown in Fig. 6.12b, where the circles correspond to the VI and the dash-dotted line corresponds to the NI approximations. Again, there is a very good agreement with the analytical results (solid line).

These results were compared to the polychromatic extraction efficiency ($\eta_{\text{extr}}^{\text{poly}}$) taking into account the lineshape of the QWs, which was calculated analytically from Eq. (A.19) and represented in Fig. 6.12b by the full squares. The polychromatic $\eta_{\text{extr}}^{\text{poly}}$ is very similar to the monochromatic results which is due to the peaked QW emission at the center wavelength (variance σ^2 is small compared to the center wavelength). The polychromatic extraction efficiency to air $\eta_{\text{extr}}^{\text{poly},0}$ (corresponding to 0 nm of metal contact) agrees well with the monochromatic η_{extr}^0 calculated at the center wavelength of the QW linewidth.

Appendix B: Sensitivity of Model to LED Parameters

We present in this section, the investigation of the sensitivity of the calculated extraction efficiency to LED parameters, revealing that for large range of LED thicknesses and QW positions within the LED, the extraction efficiency through the top facet does not change significantly. Indeed the estimation of the extraction efficiency is mostly, if not solely, affected by the metal contact properties. Moreover, the sensitivity of our model to different metal contacts is presented, which shows that the appropriate choice of metal contacts reduces significantly the dependence of the modelling results on the LED parameters.

Let us first present the effect of the LED thickness on the calculated extraction efficiency η_{extr} . Figure 6.13a shows the η_{extr} of a GaN LED on sapphire substrate for $\lambda = 445$ nm, where the QW is positioned at a fixed 140 nm distance from the top surface. Four cases of metal contacts are considered: no metal, Au, Ag and Al, where the metal thickness is 15.4 nm. In all cases, the extraction efficiency oscillates significantly for an LED structure thinner than 1 μm , and tends to a fixed value for thicker structures. In practical LEDs, the fast oscillating behavior shown in Fig. 6.13a is averaged due to thickness fluctuations and polychromatic emission from the source which yields a much smoother function almost independent on LED thickness. Suffice to notice that the half period of such oscillations is ~ 50 nm for a fixed $\lambda = 445$ nm, which is much shorter than the thickness fluctuations present in real devices. A more general map of the extraction efficiency is shown in Fig. 6.4b, where an LED structure without metal contacts was considered, showing that the extraction efficiency η_{extr}^0 is fairly constant for thick LED structures.

Let us investigate the effect of the LED parameters on the total power emitted from the source inside the LED cavity. In the models presented in this chapter, the

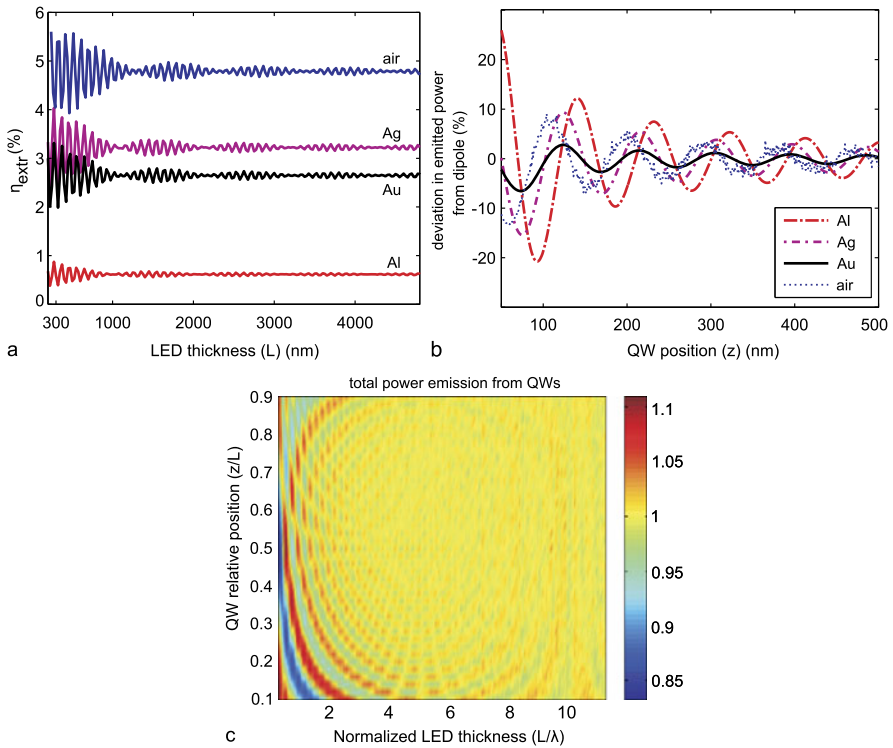


Fig. 6.13 (a) Extraction efficiency as a function of LED thickness for a QW positioned at a fixed 140 nm from the top surface for four cases of metal contacts: no metal, Au, Ag and Al and all metals are 15.4 nm-thick. (b) Deviation from unity of total radiated power by the source within the LED as a function of the QW position for the same metals. (c) Total radiated power by the dipole source inside the LED as a function of LED thickness and QW position

dipole terms were normalized to yield a unity emitted power in a homogeneous medium. When these dipoles are placed inside the LED heterogeneous medium, or in an optical cavity, the total power emitted from the dipole source may vary because its amplitude is kept constant but the optical medium is modified. This effect is related to a change in radiative emission rate from a source within an optical cavity, or Purcell effect [30]. One assumption made in our models was that the total emitted power from the dipole sources inside the LED would be considered unity due to a negligible Purcell effect in common LED structures.

Here, we test this assumption by calculating the deviation from unity of the total emitted power by the dipole sources inside the LED cavity. Let us consider the effect of the most sensitive LED parameter which is the distance of the QWs to the top surface. The deviation of the total emitted power from unity by the dipole sources inside the LED structure calculated as a function of the QW distance to the top surface z for a total LED thickness of 4729 nm is shown in Fig. 6.13b. The same four cases of metal contacts are considered: no metal, Au, Ag and Al, where the

metal thickness is 15.4 nm and it is interesting to notice that the metal contact plays a significant role in this case.

The deviation from unity in total emitted power due to a cavity effect can be significantly reduced by judiciously choosing the metal contacts, for example in the case of Au, it is at most 2 % for realistic LED structures ($z > 150$ nm). In case other metals such as Al or Ag are used as contacts, the deviation given in this plot can be used as a corrective factor for the theoretical extraction efficiency. The total emitted power tends to unity as the QW is placed farther from the LED top surface. While the oscillations observed in Fig. 6.13b are only slightly averaged to the polychromatic emission from the source, the use of several QWs or thick active regions, as well as thickness fluctuations of the LED structure, average these oscillations resulting in a smaller deviation of the emitted power from unity.

A more general map of the deviation from unity of the power emitted from the dipole sources inside the LED is shown in Fig. 6.13c, where an LED structure without metal contacts was considered. As can be seen, the total emission from the dipole source is fairly constant for a thick LED structure ($(L/\lambda) > 5$).

Therefore, under appropriate choice of metal contacts, the technique presented in this chapter is robust to LED parameters and the results presented in Sect. 6.3.1, or more specifically shown in Fig. 6.4 can be generally applied to a large range of LED configurations.

Appendix C: Modelling the Angle-Resolved Emission from LEDs: Accounting for Surface Roughness

The model presented in this chapter (details in Appendix A) can be used to predict the angular emission of an LED structure, as shown in Fig. 6.6. In particular, it is useful to check whether light emission occurs according to theoretical predictions. The power per solid angle of an LED can be experimentally measured using an angle-resolved setup [31] and compared to the theoretical angle-resolved emission, as demonstrated in Ref. [14]. The light radiated to air from the LED structure corresponds to $dP_{\text{out}}^{(h,\text{total})}/d\Omega dS(\theta) = dP_{\text{out}}^{(h,\text{TE})}/d\Omega dS + dP_{\text{out}}^{(h,\text{TM})}/d\Omega dS$. To compare this angular power flow to the corresponding angle-resolved measurement, a correction term $\cos(\theta)$ needs to be used to take into account the projection of the power flow (perpendicular to the LED top surface) into the plane perpendicular to the rotating detector.

Figure 6.14a shows the radiation from the LED (total power per solid angle) versus θ and λ , where the oscillations observed correspond to the Fabry-Perot interferences on the interfaces of the LED structure. While experimental results for LEDs with flat surface match such angular emission (Fig. 6.6a), LEDs with rough surface or pits present diminished oscillations in their angular diagram. The effect of surface roughness can be considered as a damping on the Fabry-Perot oscillations through the assumption that the roughness randomizes the angular distribution of the power flow. Therefore, a fraction F_{rough} of the original power flow is now randomly emitted in all angles, which can be approximated by an isotropic emission

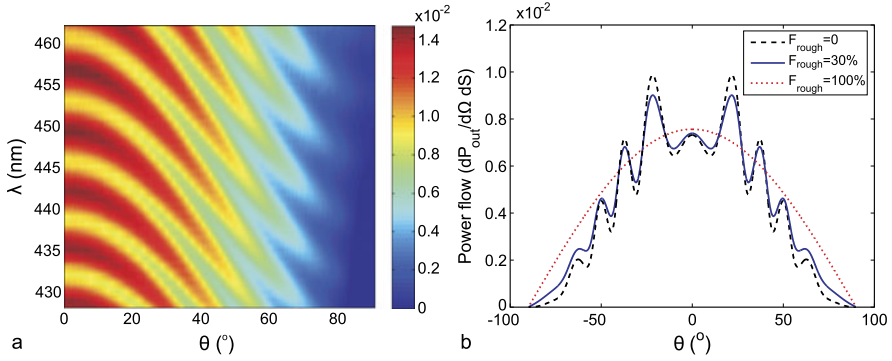


Fig. 6.14 (a) Theoretical angle-resolved radiation ($dP_{\text{out}}^{(h,\text{total})}/d\Omega dS$) versus θ (for θ from 0° to 90°) and λ showing the Fabry-Perot interferences at the interfaces of the LED structure. The LED structure consisted of a $4.87 \mu\text{m}$ -thick GaN with QW embedded at 140 nm below the top surface. (b) Effect of surface roughness on the angular power flow, normalized by the total power emitted to air, for a smooth LED with $F_{\text{rough}} = 0$ (dashed line), for $F_{\text{rough}} = 30\%$ (solid line) and for $F_{\text{rough}} = 100\%$ (dotted line)

normalized by the total power emitted to air η_{extr} , as $R = \eta_{\text{extr}}/2\pi$. A more rigorous investigation of the effect of rough surfaces is presented in Refs. [32, 33]. The normalized angular output power flow due to the rough surface is approximated by

$$\frac{F_{\text{rough}}R + (1 - F_{\text{rough}})dP_{\text{out}}^{(h,\text{total})}/d\Omega dS}{\eta_{\text{extr}}} \quad (\text{C.1})$$

Fig. 6.14b illustrates this effect, where the dashed line is the corrected angular power flow, normalized by the total power emitted to air, for a smooth LED with $F_{\text{rough}} = 0$. The solid line corresponds to $F_{\text{rough}} = 30\%$ and the dotted line is for $F_{\text{rough}} = 100\%$. The angle-resolved measurement is a useful technique to assess the contribution of light randomly scattered at rough surfaces to the measured EQE, which ultimately can be used to validate the model requirements of flat interfaces. The pronounced Fabry-Perot oscillations in this measurement fade with increase of F_{rough} which largely reduces the accuracy of this model.

References

1. I. Schnitzer, E. Yablonovitch, C. Caneau, T.J. Gmitter, Appl. Phys. Lett. **62**, 131 (1993)
2. M.R. Krames, M. Ochiai-Holcomb, G.E. Hoffer, C. Carter-Coman, E.I. Chen, I.-H. Tan, P. Grillot, N.F. Gardner, H.C. Chui, J.-W. Huang, S.A. Stockman, F.A. Kish, M.G. Craford, T.S. Tan, C.P. Kocot, M. Hueschen, J. Posselt, B. Loh, G. Sasser, D. Collins, Appl. Phys. Lett. **75**, 2365 (1999)
3. M. Yamada, T. Mitani, Y. Narukawa, S. Shioji, I. Niki, S. Sonobe, K. Deguchi, M. Sano, T. Mukai, Jpn. J. Appl. Phys. **41**, L1431 (2002)
4. J.J. Wierer, M.R. Krames, J.E. Epler, N.F. Gardner, M.G. Craford, J.R. Wendt, J.A. Simmons, M.M. Sigalas, Appl. Phys. Lett. **84**, 3885 (2004)

5. I. Schnitzer, E. Yablonovitch, C. Caneau, T.J. Gmitter, A. Scherer, *Appl. Phys. Lett.* **63**, 2174 (1993)
6. T. Fujii, Y. Gao, R. Sharma, E.L. Hu, S.P. DenBaars, S. Nakamura, *Appl. Phys. Lett.* **84**, 855 (2004)
7. S. Watanabe, N. Yamada, M. Nagashima, Y. Ueki, C. Sasaki, Y. Yamada, T. Taguchi, K. Tadatomo, H. Okagawa, H. Kudo, *Appl. Phys. Lett.* **83**, 4906 (2003)
8. A. Laubsch, M. Sabathil, J. Baur, M. Peter, B. Hahn, *IEEE Trans. Electron Devices* **57**, 1 (2010)
9. J. Piprek, *Semiconductor Optoelectronic Devices: Introduction to Physics and Simulation* (Academic Press, San Diego, 2003)
10. A. Hangleiter, D. Fuhrmann, M. Grewe, F. Hitzel, G. Klewer, S. Lahmann, C. Netzel, N. Riedel, U. Rossow, *Phys. Status Solidi A* **201**, 2808–2813 (2004)
11. M. Peter, A. Laubsch, P. Stauss, A. Walter, J. Baur, B. Hahn, *Phys. Status Solidi C* **5**(6), 2050 (2008)
12. A. David, M.J. Grundmann, J.F. Kaeding, N.F. Gardner, T.G. Mihopoulos, M.R. Krames, *Appl. Phys. Lett.* **92**(5), 053502 (2008)
13. E. Matioli, C. Weisbuch, *J. Appl. Phys.* **109**, 073114 (2011)
14. A. Getty, E. Matioli, M. Iza, C. Weisbuch, J. Speck, *Appl. Phys. Lett.* **94**(18), 181102 (2009)
15. S.G. Tikhodeev, A.L. Yablonskii, E.A. Muljarov, N.A. Gippius, T. Ishihara, *Phys. Rev. B* **66**(4), 045102 (2002)
16. P. Kivisaari, L. Riuttanen, J. Oksanen, S. Suihkonen, M. Ali, H. Lipsanen, J. Tulkki, *Appl. Phys. Lett.* **101**, 021113 (2012)
17. Y.C. Shen, G.O. Mueller, S. Watanabe, N.F. Gardner, A. Munkholm, M.R. Krames, *Appl. Phys. Lett.* **91**, 141101 (2007)
18. M. Born, E. Wolf, *Principles of Optics* (Cambridge University Press, Cambridge, 2000)
19. L.A. Coldren, S.W. Corzine, *Diode Lasers and Photonic Integrated Circuits* (Wiley, New York, 1995)
20. E.D. Palik, *Handbook of Optical Constants I* (Academic Press, San Diego, 1985)
21. A. Getty, PhD thesis, UCSB (2009)
22. H. Benisty, H. De Neve, C. Weisbuch, *IEEE J. Quantum Electron.* **34**, 9 (1998)
23. E. Matioli, B. Fleury, E. Rangel, E. Hu, J.S. Speck, C. Weisbuch, *J. Appl. Phys.* **107**, 053114 (2010)
24. R. Windisch, P. Altieri, R. Butendeich, S. Illek, P. Stauss, W. Stein, W. Wegleiter, R. Wirth, H. Zull, K. Streubel, *Proc. SPIE* **5366**, 43 (2004)
25. H. Benisty, R. Stanley, M. Mayer, *J. Opt. Soc. Am. A* **15**, 1192–1201 (1998)
26. J.P. Weber, S. Wang, *IEEE J. Quantum Electron.* **27**, 2256 (1991)
27. S.L. Chuang, C.S. Chang, *Phys. Rev. B* **54**(4), 2491 (1996)
28. S.L. Chuang, *Physics of Photonic Devices* (Wiley, New York, 2009)
29. D. Ochoa, PhD thesis, EPFL (2000)
30. E.M. Purcell, H.C. Torrey, R.V. Pound, *Phys. Rev.* **69**, 37–38 (1946)
31. A. David, C. Meier, R. Sharma, F.S. Diana, S.P. DenBaars, E. Hu, S. Nakamura, C. Weisbuch, H. Benisty, *Appl. Phys. Lett.* **87**(10), 101107 (2005)
32. G. Lerondel, R. Romestain, *Appl. Phys. Lett.* **74**, 2740 (1999)
33. J.M. Elson, J.P. Rahn, J.M. Bennett, *Appl. Opt.* **19**, 669 (1980)